sciendo

POLISH MARITIME RESEARCH 3 (119) 2023 Vol. 30; pp. 12-21
10.2478/pomr-2023-0035

MODELLING OF LAKE WAVES TO SIMULATE ENVIRONMENTAL DISTURBANCE TO A SCALE SHIP MODEL

Andrzej Rak*
Anna Miller
Gdynia Maritime University, Faculty of Electrical Engineering, Department of Ship Automation, Gdynia, Poland,

* Corresponding author: *a.rak@we.umg.edu.pl (Andrzej Rak)*

ABSTRACT

In the development of ship motion control systems, software simulations or scale model experiments in pools or open water are very often carried out in the verification and testing stages. This paper describes the process of building a software wave simulator based on data gathered on the Silm Lake near Iława, Poland, where scale ship models are used for research and training. The basis of the simulator structure is a set of shaping filters fed with Gaussian white noise. These filters are built in the form of transfer functions generating irregular wave signals for different input wind forces. To enable simulation of a wide range of wind speeds, nonlinear interpolation is used. The lake wave simulation method presented in this paper fills a gap in current research, and enables accurate modelling of characteristic environmental disturbances on a small lake for motion control experiments of scale model ships.

Keywords: wave modelling, environmental disturbances, scale ship model, ship motion simulation

INTRODUCTION

One of the main developments that seems likely to change the *modus operandi* of the global transportation system the most over the coming decades involves autonomous vehicles, including maritime shipping [21]. When designing an autonomous seagoing vessel, one vital factor is the motion control system for all phases of the cruise, from berth to berth. For a fully autonomous ship, this type of voyage will include port manoeuvres, as well as moving in restricted water areas at low speeds. Under such conditions, it is crucial to take into account the impact of environmental disturbances when designing the control system to ensure that these manoeuvres are fully safe [7].

Except for software simulations, research projects in this area typically include the testing and verification of control systems using scale model ships sailing in open waters, such as lakes or ponds [1, 3, 15, 20]. A model of the environmental load on a scale ship caused by waves and wind blowing over a small inland lake is therefore needed. Unfortunately, the currently available models of environmental disturbance, which are widely used for simulations of marine control systems, are equivalent to fully developed ocean or open sea conditions [6, 18]. Existing research on the description of lake waves has used several different types of models, and has focused mostly on geophysical and environmental issues [2, 9]. This work describes the process of designing a unidirectional, nonlinear wave model that is suitable for simulating the influence of a lake surge on a scale ship. Source data for the project were collected from the Silm Lake, Poland, which is used as a research area for the manoeuvring of scale ships [17]. Introductory analyses of the wind and wave phenomena in this location have been reported in previous papers by the current authors [12, 13]. A corresponding elaboration of a wind model is being prepared for a separate publication.

MODELLING OF THE WAVE SIGNAL

Sea waves can be described as a stationary random process [5], and the reconstruction of these waves can be achieved by appropriate shaping of the frequency components of a continuous standard input signal. Of the shaping methods in the literature [10], the most commonly used for this purpose are filters implemented in the form of approximate state-space structures, convolution filters with directly specified power spectral densities (PSDs), or compositions of orthogonal basis functions, typically cosine ones, which directly correspond to the PSD, with variable phase shifts or amplitudes at the boundary of the periodic signal. Shaping filters are usually designed as linear time-invariant (LTI) systems driven by white noise. These give good simulation performance, and a suitable PSD approximation assuming correctly identified the LTI system. Based on the ITTC guidelines [18], it was decided in this project to model wave PSDs as an LTI system.

It is known that the PSD of a Gaussian white noise signal (GWN) is equal to:

$$S_x(f) = \frac{N_0}{2} \tag{1}$$

for all frequencies f. An LTI system is characterised in the time domain by the impulse response:

$$h(t) = T[\delta(t)], \tag{2}$$

where $\delta(t)$ is a Dirac delta function. The output signal $y(t)$ of the filter may be determined as the convolution of an LTI system impulse response with a GWN input signal $x(t)$:

$$y(t) = h(t) * x(t). \tag{3}$$

Since $x(t)$ is a GWN random signal, the system output $y(t)$ is also a Gaussian process. Hence, for a discrete system, the output signal can be defined as:

$$y_n = \sum_k h_k \, x_{n-k}, \tag{4}$$

where n is the sample number, and k is the time shift. An LTI system transfer function is defined as:

$$H(f) = \sum_n h_n \, e^{-j2\pi nf}. \tag{5}$$

Taking into account Eq. (3) in the frequency domain, the desired frequency component $\hat{Z}(f)$ corresponding to the measured wave spectrum $Z(f)$ can be expressed as:

$$\hat{Z}(f) = H(f)W(f), \tag{6}$$

where $W(f)$ is a white noise spectrum. Hence, the power density function to be realised is given by:

$$S_z(f) = |H(f)|^2 S_x(f) = |H(f)|^2 \frac{N_0}{2}. \tag{7}$$

In the relationship above, the PSD can be approximated by a suitable transfer function, which can be computed from the PSD for a measured wave, $S_w(f)$, using the least squares method (LSM) as follows:

$$\min_{a_k, b_m} \sum_{j=1}^{m} \left(|H(j2\pi f)| - \sqrt{\left(S_w(j2\pi f)\right)^2} \right), \tag{8}$$

where a_k, b_m are LTI filter coefficients, $H(2\pi f)$ is the desired frequency response, and $m \geq k$. The corresponding discrete filter transfer function with sample time corresponding discrete filter transfer function with sample time $T_s = 0.1$ [s] can be calculated as follows:

$$H(z) = \sum_{n=-\infty}^{+\infty} h\,(n) z^{-n}, \tag{9}$$

and has the form:

$$H(z) = \frac{a_0 + a_1 z^{-1} + \ldots + a_p z^{-p}}{1 + \left(b_1 z^{-1} + \ldots + b_q z^{-q}\right)}. \tag{10}$$

A corresponding analogue filter, which reproduces the wave parameters, can be designed based on the assumptions of the bilinear transformation method. The following function [8] can be used to convert a digital filter with transmittance $H(z)$ to an analogue filter with transmittance $H(s)$:

$$z = \phi(s) = \frac{1 + s\frac{T_s}{2}}{1 - s\frac{T_s}{2}}, \tag{11}$$

where T_s is the discrete signal sampling time. Finally, the resulting LTI object can be obtained in the form of a transfer function:

$$T(s) = k\frac{b_n s^n + \dots + b_1 s + b_0}{a_m s^m + \dots + a_1 s + a_0}. \quad (12)$$

DESIGN OF A LAKE WAVE DIGITAL SIMULATOR

A lake wave simulator was designed based on the assumption that all waves are generated by winds. The structure of our simulator is shown in Fig. 1, where the mean wind speed v_w [m/s] is the input value, and the wave height h_w [mm] is the output signal.

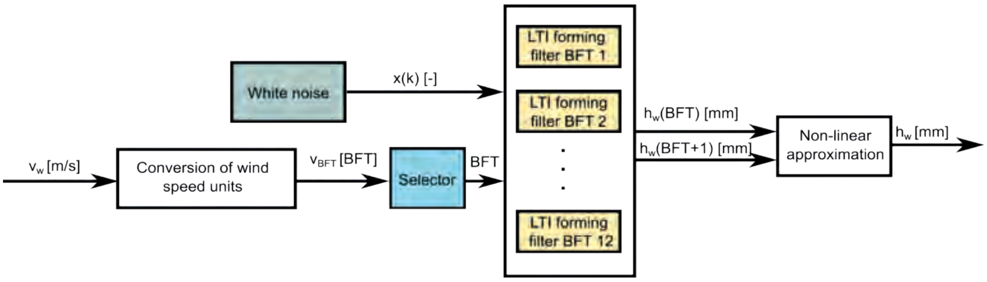

Fig. 1. Block diagram of the wave generation algorithm

A white noise generator is used as a signal source. A noise seed can be defined rather than a random selection of parameters, which leads to reproducible results from the wave signal specification. The "Selector" module rounds the force of the wind to the integers on the Beaufort wind scale (BFT), and acts as a switch for the appropriate pair of LTI forming filters. The wind speed is recalculated based on the BFT at the scale of the ship model to avoid confusion from an assessment of the wind impact based on two different reference measures in metres per second caused by the scaling of the ship. The transformation of wind speed v_w to BFT is done using the empirical formula [11]:

$$v_{BFT} = 1.42\left(v_w\sqrt{1/sc}\right)^{0.61}, \quad (13)$$

where sc is the model scale (sc = 1:24); v_{BFT} is the wind force in BFT, proportional to the ship's scale; and v_w is the wind speed in [m/s]. The relationship between wind speed and BFT force at the scale of the ship, and a comparison with the reference points given in [6], is shown in Fig. 2.

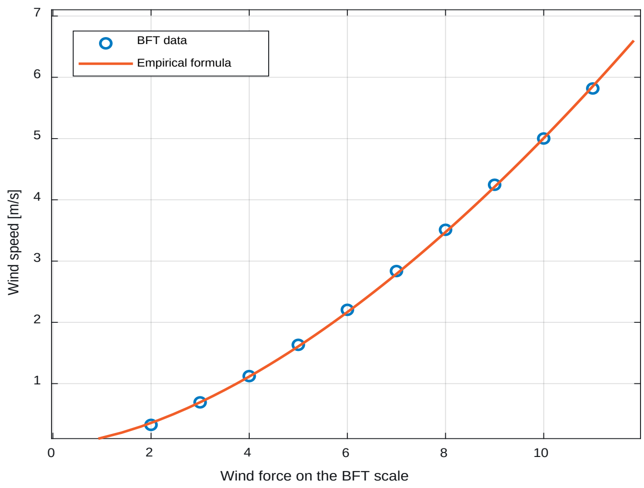

Fig. 2. Wind force [BFT] at the scale of the model ship

The wind speed at the scale of the model corresponding to the 0–1 BFT range caused no measurable wave effects on the surface of the lake, and the curve shown above therefore begins at 1 BFT. Interpolation between the outputs of the two consecutive forming filter blocks (see Fig. 1) used nonlinear weighting functions, and is described in the next section.

Measurements were taken with a device consisting of two ultrasonic anemometers, a wavemeter and a data recording computer working in real time. Details of the measurement equipment can be found in [12-14]. Data from all three instruments were acquired at a sampling rate of 10 Hz. The software was developed using the Real-Time Target Toolbox of the MATLAB package, as well as low-level functions coded in C.

EXTRAPOLATION OF RESULTS AND DEPENDENCY ANALYSIS OF WAVE HEIGHT AND WIND SPEED

Wave height and wind speed measurements were collected in several sessions between the spring of 2019 and the autumn of 2021. The measuring equipment was located on the Silm Lake, and each measurement session lasted 12 h. Detailed analyses of the acquired data and the results of spectrum modelling have been presented in [13]. The results of these studies confirmed that the wave height on a lake is strongly correlated with the wind speed. The distributions of the height deviations from the mean value and the wave amplitude were Gaussian and Rayleigh, respectively, and the wave PSD function was analogous to the ITTC formulation for the sea waves spectrum. These factors formed the basis for the construction of a digital wave simulator. The measured wave spectrum was modelled as a scaled ITTC spectrum [18] as follows:

$$s(\omega) = A\omega^{-5}exp(-B\omega^{-4}), \quad (14)$$

where:

$$A = 1.51\frac{\bar{H}_{1/3}^2}{\bar{T}_z^4}, \tag{15}$$

$$B = 105.44\bar{T}_z^4, \tag{16}$$

and $\overline{H}_{1/3}$ [mm] is the mean of the significant wave height, and $\overline{T}_z$ [s] is the mean of the significant wave period. Based on the measured values of $\overline{H}_{1/3}$ and $\overline{T}_z$ for wind forces of 4, 5, 6, 7 and 9 BFT, dependencies for $\overline{H}_{1/3}(BFT)$ and $\overline{T}_z(BFT)$ were extrapolated to obtain continuous relationships. These are shown in Figs. 3 and 4, respectively.

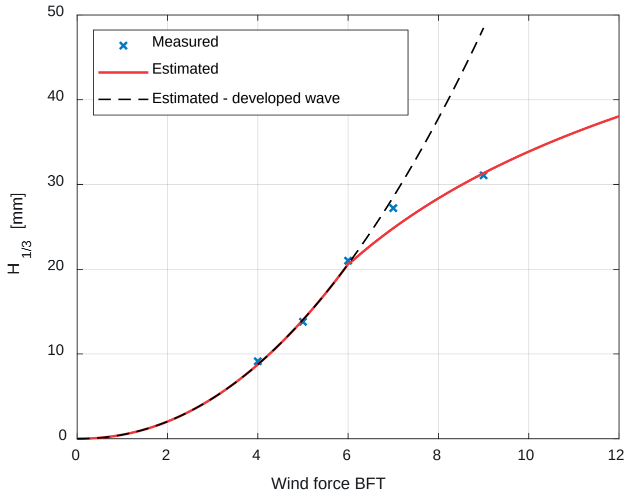

Fig. 3. Dependency of the significant wave height on the wind force

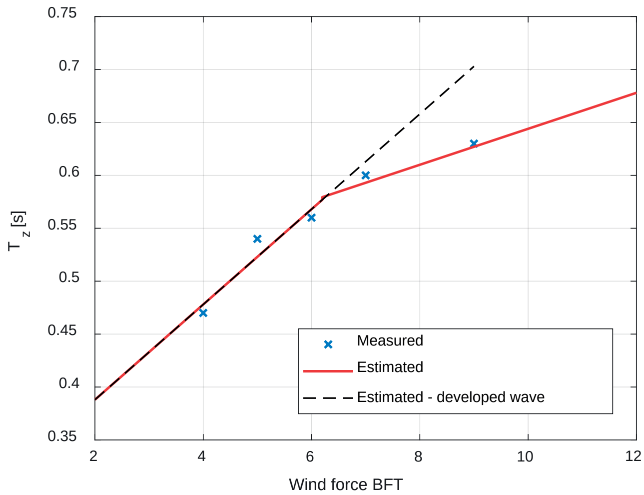

Fig. 4. Dependency of the significant wave period on the wind force

The dependence of the significant wave height on the wind speed, for fully developed sea waves, is described by a second-order polynomial [19]. The same dependence for Lake Erie is described by the square function for wind speeds between zero and 15 m/s and for higher wind speeds it is linear [4], due to the limited depth of the lake. On the Silm Lake, fully developed waves were observed for winds less than or equal than 6 BFT at the scale of the ship, and above this value, a characteristic flattening was observed (see Fig. 3). The dependence of the significant wave height on the BFT scale can be expressed as:

$$\hat{H}_{1/3} = \begin{cases} 0.47v_{BFT}^{2.11} & \text{for} \quad v_{BFT} \leqslant 6BFT \\ -149.4v_{BFT}^{-0.38} + 96.16 & \text{for} \quad v_{BFT} > 6BFT. \end{cases} \tag{17}$$

For fully developed sea waves, the dependence of the significant wave priod on the wind speed is linear [16]. For the waves measured on Silm Lake, consistency with this general rule was observed for wind forces not exceeding 6 BFT at the scale of the ship, in the same way as for the wave heights. Above this value, due to the restricted area and depth of the lake, characteristic flattening was observed, as shown in Fig. 4. The dependence of the significant wave period on scaled BFT is described by:

$$\hat{T}_z = \begin{cases} 0.045v_{BFT} + 0.298 & \text{for} \quad v_{BFT} \leqslant 6BFT \\ 0.017v_{BFT} + 0.474 & \text{for} \quad v_{BFT} > 6BFT. \end{cases} \tag{18}$$

These dependencies were estimated using an LSM curve fitting, with the fit factors shown in Table 1.

Tab. 1. Accuracy of significant wave height and period estimates

	$\hat{T}_z$ [Hz]		$\hat{T}_{1/3}$ [mm]	
	$v_{BFT} \leq 6$ [BFT]	$v_{BFT} > 6$ [BFT]	$v_{BFT} \leq 6$ [BFT]	$v_{BFT} > 6$ [BFT]
R^2	0.813	0.923	0.996	0.992
RMSE	0.024	0.011	0.510	1.110

NONLINEAR WAVE HEIGHT APPROXIMATION

The wave generator structure shown in Fig. 1 requires a selector for the consecutive reconstruction filters designed for each BFT. To obtain a continuous wave height signal, interpolation is required between the outputs of the selected filters. This interpolation is done based on a sigmoid function:

$$\Delta h_{coeff}(\Delta BFT) = 1 - \frac{1}{1+e^{5(1-\Delta BFT)}}, \tag{19}$$

where Δh_{coeff} is the forming filter output multiplier, and ΔBFT is the difference between the mean wind speed value (recalculated to the BFT scale for the ship) and the next integer on the BFT scale.

The shape of this nonlinear function is shown in Fig. 5.

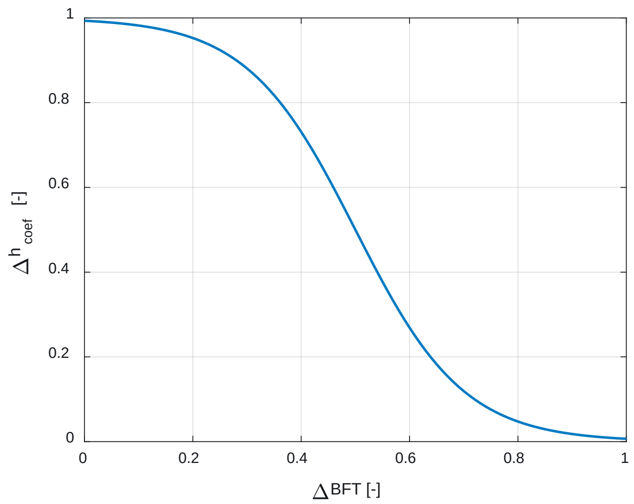

Fig. 5. Nonlinear wave height interpolation function

RESULTS

The workflow described in the section entitled "Modelling of the Wave Signal" was applied to the design of a digital wave generator. The MATLAB-Simulink package was used as a software development environment, and the parameters of the scaled ITTC spectrum (see Eqs. (15) and (16)) were calculated using the estimated significant wave height and period for each point on the BFT scale.

DESIGN OF THE FORMING FILTERS

Twelve IIR forming filters were designed, for which the parameters were estimated using the LSM optimisation in Eq. (8). These IIR filter factors were stored in second-order section (SOS) matrices and used to determine the parameters for the discrete transfer functions. In the real world, wave height is modelled as a continuous analogue signal, and to remain consistent with this assumption, continuous transfer functions were computed as shown in Eq. (12). A decision was made to keep the order of the filter transfer functions as low as possible, at the cost of an acceptable level of simulator inaccuracy. A second-order transfer function of general form was therefore proposed as follows:

$$T(s) = k\,\frac{b_2 s^2 + b_1 s + b_0}{a_2 s^2 + a_1 s + a_0}. \qquad \textbf{(20)}$$

The values of the filter coefficients a, b and k (gain) for each point on the BFT scale are shown in Table 2.

Tab. 2. Coefficients for filter transfer functions

BFT	k	b_2	b_1	b_0	a_2	a_1	a_0
2	14	0.0065	0.034	$2.4{\cdot}10^{-5}$	1	2.35	161.5
3	6.4	0.36	0.22	0.011	1	2.45	138.1
4	3.2	0.074	0.51	0.0031	1	2.10	116.1
5	3	0.22	1.74	0.028	1	1.86	87.12
6	1.7	0.59	4.83	0.026	1	1.92	80.65
7	1.1	1.02	8.59	0.20	1	1.67	69.44
8	0.6	2	17.00	1.08	1	1.51	65.89
9	0.82	1.47	12.54	0.30	1	1.50	63.52
10	0.75	1.93	16.77	0.13	1	1.54	58.44
11	0.78	1.20	17.57	0.15	1	1.54	56.44
12	0.83	2	17.81	0.024	1	1.58	55.00

Using the nonlinear interpolation mechanism described in the previous section, a system of forming filters was created to digitally model wind-generated waves on the Silm Lake. An example of the output from our digital wave simulator is shown in Fig. 6. This diagram includes three separate waveforms generated by winds of force 2, 2.5 and 3 BFT at the scale of the ship, corresponding to winds with average speeds of 0.35 m/s, 0.5 m/s and 0.7 m/s, respectively. From Fig. 6, it can be seen that the height and period of the waves increase with the wind speed; this pattern is consistent with the nature of the phenomena observed on the lake.

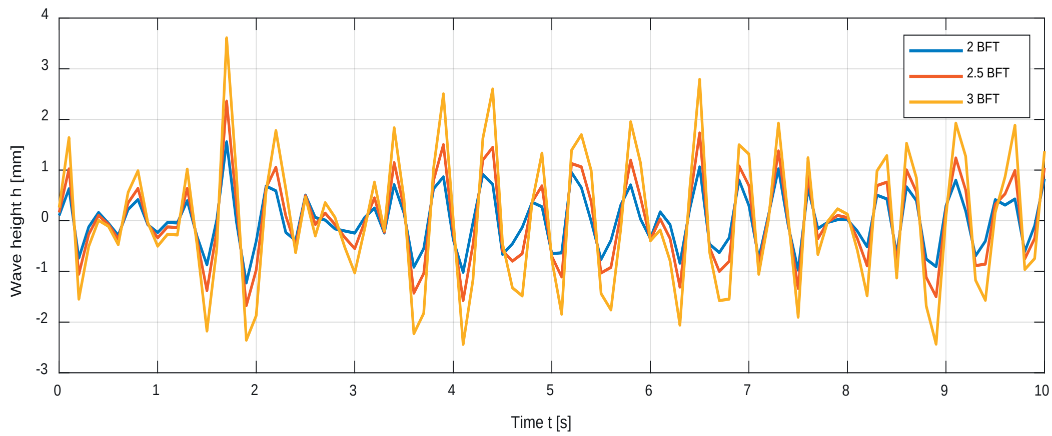

Fig. 6. Example of the output from the wave generator

A discussion of the results is presented below, and is divided into two subsections dealing with a spectral analysis of the simulated waves and their statistics.

SPECTRAL ANALYSIS OF SIMULATED WAVES

The proposed digital wave generator takes the mean value of the wind speed and a white noise signal as input, and based on these, the wave height is simulated as a function of time.

Table 3. RMSE values for the simulated spectrum

BFT [-]	2	3	4	5	6	7	8	9	10	11	12
RMSE [mm²s]	$8.18 \cdot 10^{-4}$	0.0048	0.021	0.055	0.13	0.19	0.25	0.26	0.35	0.41	0.45

The resulting values did not exceed 2% of the sum of the ITTC spectrum elements for each BFT. We therefore conclude that a high degree of convergence in the results was obtained, and that our model is sufficiently accurate to be used as a digital wave generator.

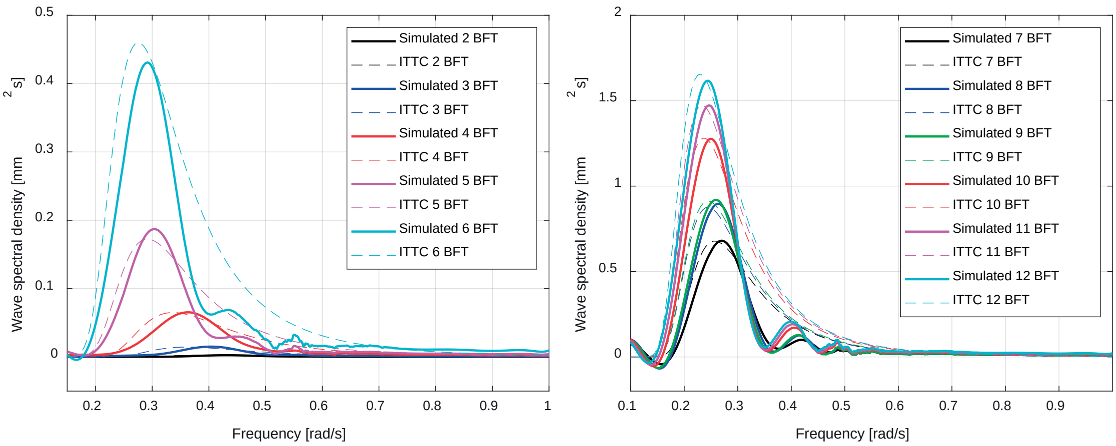

Fig. 7. Comparison of simulated and ITTC spectra

The outputs of the generator for each point on the BFT scale were compared to the standard ITTC scaled wave spectra. The results of this comparison are shown in Fig. 7, for winds of strength 2–6 BFT and 7–12 BFT. The diagram is separated into two parts to ensure readability. The simulation results are shown by the solid lines, and the corresponding ITTC spectra by the dashed lines. A high level of convergence of the results was seen over the full range of wind forces. A modal frequency shift toward lower frequencies was observed as the wind strength increased, which is consistent with the principles of ITTC spectrum modelling. The value of the wave spectral density also increased at higher points on the wind BFT scale. Moreover, narrowing of the spectrum compared with the ITTC wave spectral model was observed in the higher frequency range.

To enable a quantitative evaluation of the spectrum modelling, RMSE values were determined using the formula:

$$RMSE = \sqrt{\frac{1}{n}\sum\left(S_{ITTC}(\omega) - \hat{S}(\omega)\right)^2}, \quad \text{(21)}$$

where S_{ITTC} is the ITTC scaled standard spectrum, $\hat{S}$ is the spectrum computed on the basis of the digital generator output, and n is the number of bands in the spectrum. The values of the RMSE are listed in Table 3.

STATISTICS FOR THE SIMULATED WAVES

The mode of operation and reproduction accuracy of each filter wave were analysed separately. Based on the results of the simulation, the heights and periods of the significant waves were determined, and a statistical analysis of the obtained data was carried out. The distributions of deviations from the mean values and the distributions of the wave amplitudes were computed and compared with the distributions estimated on the basis of real measurements.

Table 4 shows the relative errors in the simulated heights and periods of significant waves for each point on the BFT scale.

Tab. 4. Relative error in the simulated wave parameters

	Measured		Simulated		Error	
BFT	$H_{1/3}$ [mm]	T_z [s]	$\hat{H}_{1/3}$ [mm]	$\hat{T}_z$ [s]	$e_{H1/3}$ [%]	e_{Tz} [%]
2	2.00	0.38	1.80	0.40	10	5.3
3	4.50	0.40	4.33	0.43	3.8	7.5
4	9.24	0.45	9.14	0.47	1.1	4.4
5	14.00	0.52	13.80	0.54	1.4	3.8
6	22.23	0.55	21.01	0.56	5.5	1.8
7	26.07	0.59	24.94	0.60	4.3	1.7
8	28.90	0.62	28.00	0.62	3.1	0
9	29.50	0.62	28.32	0.63	4	1.6
10	34.40	0.65	33.51	0.65	2.6	0
11	36.60	0.65	36.04	0.66	1.5	1.5
12	38.50	0.66	39.04	0.66	1.4	0

The mean error of the significant wave height was equal to 3.5%. The maximal value was obtained for the weakest wind force of 2 BFT, where the wave height reached 2 mm, and this value had a negligible effect on the movement of the model ship. In the other cases, the error did not exceed 5.5%. The maximal error of significant wave period reached 7.5% for winds at 3 BFT, and the mean inaccuracy of significant waves period was 2.5%. These error values indicate that the wave parameters are sufficiently well chosen to simulate the environmental disturbance generated in the motion of the ship. The distributions of the wave amplitudes and deviations from the mean values for the waves generated by weak (4 BFT), mean (6 BFT) and strong (9 BFT) winds are shown in Fig. 8. The blue bars represent data obtained from the digital generator, which are compared to the estimated distributions based on real lake measurements [13].

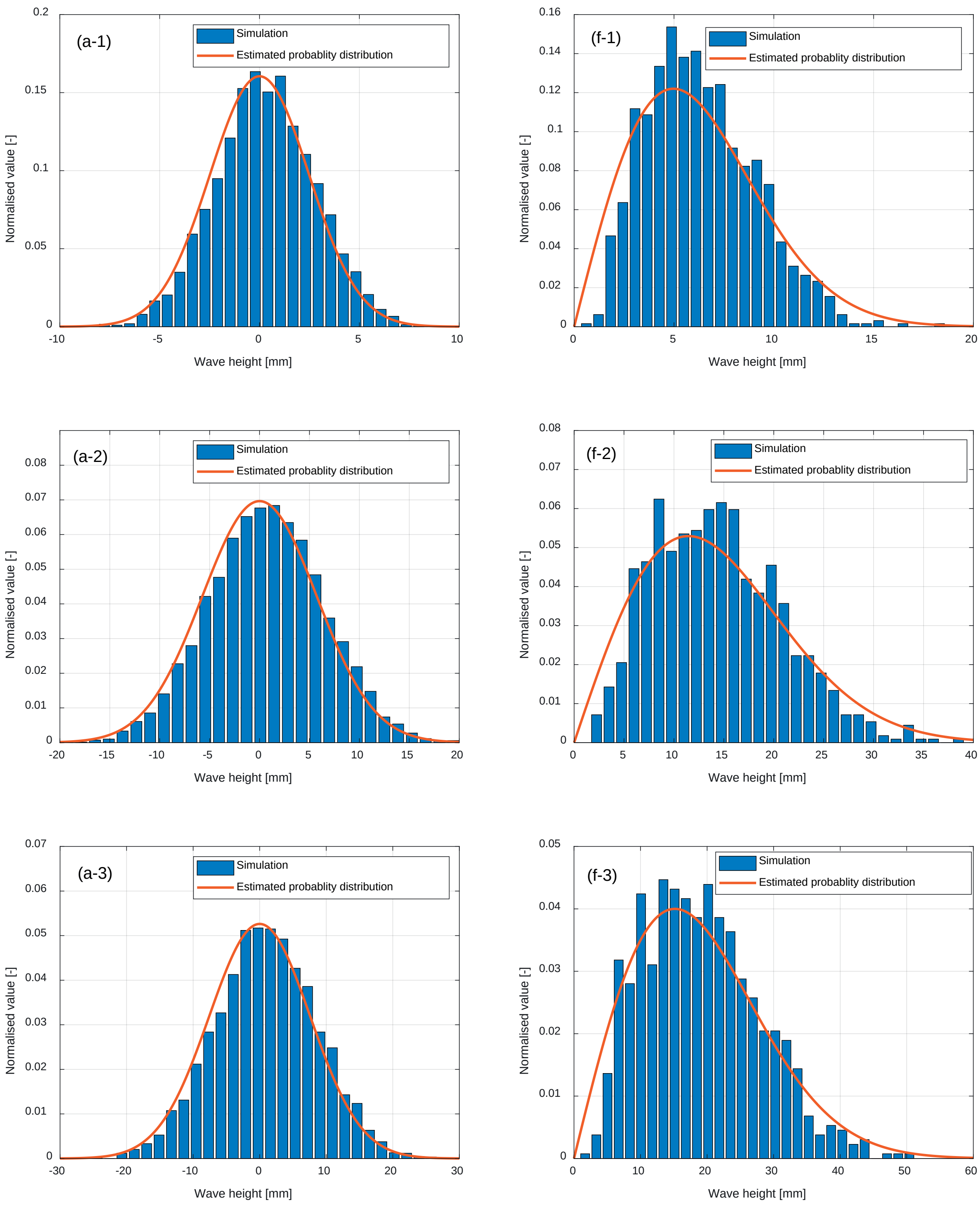

Fig. 8. Distributions of (a) wave amplitudes and (f) frequency of deviations from the mean value for (1) weak, (2) medium and (3) strong winds

The frequency of the wave height deviations from the mean value for the simulated waves had a Gaussian distribution, which coincides with the estimated probability of the wind-generated waves for each point on the BFT scale. A high level of compliance was observed for the model in this regard. All wave amplitudes were characterised by a Rayleigh distribution. The highest level of alignment with the estimation was observed for the strongest wind force (Fig. 8f-3). For a weak wind (4 BFT), the amplitudes of the generated waves were higher than expected, close to the maximum of the distribution function. In the case of a medium wind (6 BFT), a high degree of compliance was seen for the maximum of the distribution, although more waves were generated in its vicinity than expected from theory.

Fig. 9 shows examples of (a) measured and (b) digitally generated wave heights for a mean wind force of 4 BFT. Statistical parameters such as the minimal, maximal, and mean values and the standard deviation are marked by dashed lines. Their numerical values are summarised in Table 5.

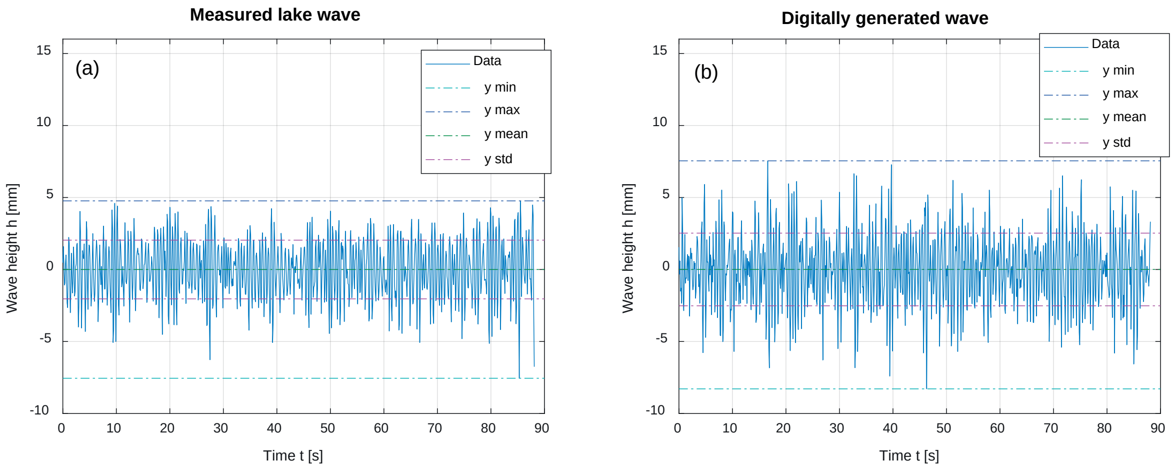

Fig. 9. Statistical parameters for waves under a wind of 4 BFT: (a) measured, (b) digitally generated

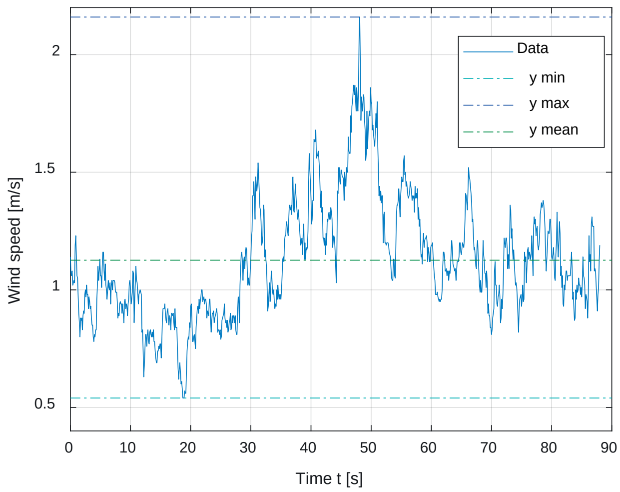

Fig. 10. Time series data for measured wind speeds

Tab. 5. Statistics for wave time histories for a wind of 4 BFT

Parameter	Measured	Simulated
Min. value [mm]	–7.55	–8.28
Max. value [mm]	4.76	7.54
Mean value [mm]	0	0
Standard deviation [mm]	2.04	2.54

In the simulation, a wave was generated under a constant mean wind speed $\overline{v}_w$ [m/s] (4 BFT), as indicated by the green dashed line in Fig. 10, while the wave measured on the lake was induced by a real, variable wind, marked on this figure by the solid line. The wind speed stabilised over the last 30 s, and the wave amplitudes in this time period varied by about 15% (0.75 mm). A difference of 25% can be observed in the standard deviation between the measured and digitally generated waves. The main reason for the difference in the amplitudes of the waves is the inconsistency in the wind causing the waves. Both wave signals are shown in Fig. 11.

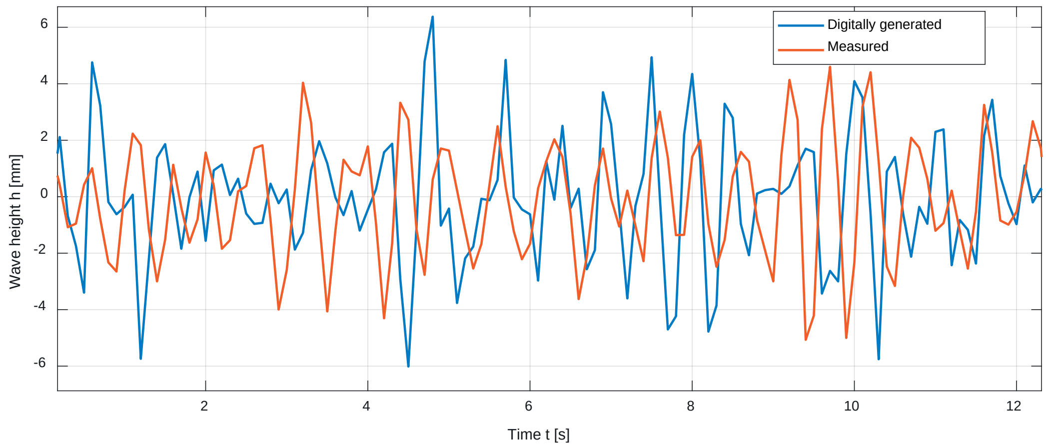

Fig. 11. Direct comparison of measured and generated waves as a function of time

In contrast, however, a distinctive similarity in the results can be seen for both the period and the amplitude. In the digitally generated signal, single waves of higher amplitude than the measured waves were observed. The data presented in Fig. 11 correspond to a wind force of 4 BFT. The occurrence of higher amplitudes is correlated with the distribution of wave amplitudes (Fig. 8f-1), where higher values for the wave heights are seen than expected from theory. The above-mentioned discrepancies do not exceed 2 mm, meaning that when modelling the external disturbances to the motion of the ship, this can be considered to have a negligible impact on the operation of the model ship.

CONCLUSIONS

The following conclusions may be drawn from the research reported in this paper:

- Based on an empirical description of the PSD of waves generated by the wind on a small lake, a digital simulator of this process could be constructed.
- The simulator consisted of a group of parallel connected shaping filters for the reconstruction of the wave signal for particular wind BFT, and was easy to implement, analyse and verify.
- The relative errors in the wave reproduction did not exceed 10%. This is an acceptable level for a wave generator for a motion control simulation of a ship.
- Unlike in open sea conditions, the dependencies of the heights and periods of significant waves on the wind force did not follow quadratic and linear relationships, respectively, for all values of force. Flattening was shown above a certain range of values.
- The time series of irregular waves generated by the simulator exhibited properties characteristic of real waves, such as a proportionally increasing height and a lengthening period as the wind strength increased.

ABBREVIATIONS USED

BFT – Beaufort wind scale
GWN – Gaussian white noise
IIR – Infinite impulse response filter
ITTC – International Towing Tank Conference
LSM – Least squares method
LTI – Linear time-invariant
PSD – Power spectral density
RMSE – Root mean square error
SOS – Second-order section

REFERENCES

1. H. L. Alfheim, K. Muggerud, M. Breivik, E. F. Brekke, E. Eide, and Ø. Engelhardtsen, "Development of a dynamic positioning system for the ReVolt model ship," IFAC-PapersOnLine, vol. 51, no. 29, pp. 116–121, Sept. 2018, doi: 10.1016/j.ifacol.2018.09.479.
2. J. C. Allan and R. M. Kirk, "Wind wave characteristics at Lake Dunstan, South Island, New Zealand," New Zeal. J. Mar. Fresh., vol. 34, no. 4, pp. 573–591, Mar. 2000, doi: 10.1080/00288330.2000.9516959.
3. A. M. Bassam, A. B. Phillips, S. R. Turnock, and P. A. Wilson, "Experimental testing and simulations of an autonomous, self-propulsion and self-measuring tanker ship model," Ocean Eng., vol. 186, pp. 106065, Aug. 2019, doi: 10.1016/j.oceaneng.2019.05.047.
4. C. Drews, "Using wind setdown and storm surge on Lake Erie to calibrate the air-sea drag coefficient," PLOS ONE, vol. 8, no. 8, pp. 1–16, Aug. 2013, doi: 10.1371/journal.pone.0072510.
5. O. M. Faltinsen, Sea Loads on Ships and Offshore Structures, Cambridge University Press, Cambridge – New York, 1990.

6. T. I. Fossen, Handbook of Marine Craft Hydrodynamics and Motion Control, John Wiley & Sons, Ltd, 2011, doi:10.1002/9781119994138.

7. W. Gierusz and M. Rybczak, "Effectiveness of multidimensional controllers designated to steering of the motions of ship at low speed," Sensors, vol. 20, no. 12, p. 3533, Jun. 2020, doi: 10.3390/s20123533.

8. T. Holton, Digital Signal Processing: Principles and Applications, Cambridge University Press, 2021, doi:10.1017/9781108290050.

9. K-R. Jin and Z-G Ji, "Calibration and verification of a spectral wind–wave model for Lake Okeechobee," Ocean Eng., vol. 28, no. 5, pp. 571–584, May 2001, doi: 10.1016/S0029-8018(00)00009-3.

10. A. Klockner, A. Knoblach and A. Hackmann, "How to shape noise spectra for continuous system simulation," Math. Comp. Model. Dyn., vol. 23, no. 3, pp. 284–300, Feb. 2017, doi:10.1080/13873954.2017.1298622.

11. J. Ley and O. el Moctar, "A comparative study of computational methods for wave-induced motions and loads," J. Mar. Sci. Eng., vol. 9, no. 1, p. 83, Jan. 2021, doi: 10.3390/jmse9010083.

12. A. Miller and A. Rak, "Measurement system for the environmental load assessment of the scale ship model," Sensors, vol. 23, no. 1, p. 306, Dec. 2022, doi: 10.3390/s23010306.

13. A. Miller and A. Rak, "A measurement system for the environmental load assessment of a scale ship model–Part II," Sensors, vol. 23, no. 7, p. 3415, Mar. 2023, doi: 10.3390/s23073415.

14. L. Morawski, J. Pomirski, P. Sikora, and R. Sokół, "Measurement system for wind and waves characteristics registration on the Silm Lake," TransNav: International Journal on Marine Navigation and Safety of Sea Transportation, vol. 4, no. 2, pp. 205–207, Jun. 2010, doi:10.1201/9780203869345.ch83

15. L. P. Perera, L. Moreira, F. P. Santos, V. Ferrari, S. Sutulo, and C. Guedes Soares, "A navigation and control platform for real-time manoeuvring of autonomous ship models," IFAC Proc. Vol., vol. 45, no. 27, pp. 465–470, 2012, doi: 10.3182/20120919-3-IT-2046.00079.

16. W. J. Pierson Jr. and L. Moskowitz, "A proposed spectral form for fully developed wind seas based on the similarity theory of S. A. Kitaigorodskii," J. Geophys. Res., vol. 69, no. 24, pp. 5181–5190, Dec. 1964, doi:10.1029/JZ069i024p05181.

17. Shiphandling Research and Training Centre. [Online]. Available: http://www.ilawashiphandling.com.pl [Accessed 15 April 2023].

18. C. T. Stansberg, G. Contento, S. Hong, M. Irani, S. Ishida, and R. Mercier, "The Specialist Committee on Waves final report and recommendations to the 23rd ITTC," In: Proceedings of the 23rd ITTC, Venice, Italy, 8–14 Sep. 2002, pp. 505–736.

19. D. N. Sugianto, M. Zainuri, A. Darari, S. S. Darsono and N. Yuwono, "Wave height forecasting using measurement wind speed distribution equation in Java Sea, Indonesia," International Journal of Civil Engineering and Technology, vol. 8, no. 5, pp. 604–619, May 2017.

20. M. Tomera, "Hybrid switching controller design for the maneuvering and transit of a training ship," Int. J. Appl. Math. Comput. Sci., vol. 27, no. 1, Mar. 2017, pp. 63–77. doi:10.1515/amcs-2017-0005.

21. A. Tsvetkova and M. Hellström, "Creating value through autonomous shipping: An ecosystem perspective," Marit. Econ. Logist., vol. 24, no. 2, pp. 255–277 Jun. 2022, doi: 10.1057/s41278-022-00216-y.